J. Mech. Phys. Solids Vol. 39, No. 2, pp. 223–241, 1991.
Printed in Great Britain.

0022-5096/91 $3.00 + 0.00

CAVITATION INSTABILITIES IN ELASTIC–PLASTIC SOLIDS

Y. HUANG, J. W. HUTCHINSON and V. TVERGAARD†

Division of Applied Sciences, Harvard University, Cambridge, MA 02138, U.S.A. and
† Department of Solid Mechanics, The Technical University of Denmark, DK-2800, Lyngby, Denmark

(*Received* 20 *November* 1989)

ABSTRACT

A CAVITATION instability occurs when an isolated void in an infinite, remotely stressed elastic–plastic solid grows without bound under no change of remote stress or strain. The cavitation instability can be thought of as a process in which elastic energy stored in the remote field drives the plastic expansion of the void. The paper begins with a brief review of cavitation under spherically symmetric stress states and then goes on to consider the problem for cavitation states under general axisymmetric stressing. It is found that the criterion for cavitation under multiaxial axisymmetric stressing depends on the attainment of a critical value of the mean stress, to a reasonably good approximation. A set of recent experiments is discussed in which cavitation instabilities appear to have occurred. The last section of the paper reviews available theoretical results for the dilatation rates of isolated voids. The most commonly used formulae underestimate the dilatation rate under stress states with moderate to high triaxiality.

1. INTRODUCTION

CAVITATION instabilities can occur when stress levels are sufficiently high such that the work made available from the field surrounding the void by its expansion is enough to drive continued expansion. A void in an infinite body grows without bound when a cavitation stress limit is reached. Thus, unlike normal void growth which occurs directly in proportion to the deformation imposed on a solid, the cavitation phenomenon addressed here is an instability which occurs at stationary remote strain. The existence of such instabilities was recognized by BISHOP *et al.* (1945) who determined cavitation limits in elastic–plastic solids under stress conditions consistent with spherical and cylindrical symmetries. HILL (1950) presents limit states for the equivalent problems of spherical and cylindrical cavities subject to internal pressure. Cavitation states have received attention in recent years in the theory of nonlinear elasticity as intrinsic material stability limits (BALL, 1982). Motivation for the present work derives from ductile failure mechanisms under highly constrained plastic flow. One example, to be discussed in the paper, is the cavitation failure mode in a ductile wire reinforcing a brittle matrix observed by ASHBY *et al.* (1989). Cavitation also appears to be a likely failure mechanism in a thin ductile metal layer used to bond two ceramic blocks together (DALGLEISH *et al.*, 1989). The constraint of the ceramic materials, which do not deform plastically, gives rise to very high levels of stress

triaxiality in the metal layer. It is under very high stress triaxiality that cavitation instabilities occur.

To set the stage for work in this paper on cavitation states under general axisymmetric remote stressing, we begin by briefly reviewing the analysis and results for cavitation of spherical voids subject to remote hydrostatic tension. Earlier treatments for this particular loading can be found in the papers by CHADWICK (1959) and DURBAN and BARUCH (1976). Recent studies of the spherically symmetric problem have included the effect of material rate-sensitivity on cavitation (ABEYARATNE and HOU, 1989), and the effect of material inertia coupled with transient loading (ORTIZ and MOLINARI, 1989).

2. SPHERICALLY SYMMETRIC CAVITATION STATES

We begin by considering an isotropic, incompressible elastic–plastic solid with a uniaxial relation between true stress and logarithmic strain given by

$$\sigma/\sigma_Y = f(\varepsilon), \tag{2.1}$$

where σ_Y is some convenient choice of tensile yield stress. Let ρ denote the distance of a material point from the center of the spherical cavity in the undeformed state with R_i as the radius of the cavity. Let R be the distance of the same material point from the center of the cavity in the current state and let R_0 be the deformed radius of the cavity. By incompressibility, the logarithmic radial and hoop strains of the material element currently at R are

$$\varepsilon_R = -2\varepsilon_\theta = \frac{2}{3}\ln[1-(R_0^3-R_i^3)/R^3]. \tag{2.2}$$

With $\sigma_R(R)$ and $\sigma_\theta(R)$ denoting the true stress components in the current configuration at R, equilibrium requires

$$\frac{d\sigma_R}{dR} + \frac{2}{R}(\sigma_R-\sigma_\theta) = 0 \tag{2.3}$$

together with the boundary conditions

$$\sigma_R = 0, \quad R = R_0 \quad \text{and} \quad \sigma_R \to \sigma^\infty \quad \text{as } R \to \infty. \tag{2.4}$$

By superposition of hydrostatic pressure, one can convert the stress state $(\sigma_R, \sigma_\theta, \sigma_\theta)$ to an equivalent uniaxial state $\sigma_R-\sigma_\theta$. Thus, $(\sigma_R-\sigma_\theta)/\sigma_Y = f(\varepsilon_R)$, which is on the compression side of the uniaxial curve since ε_R is negative when the void is expanding. It is assumed that R_0/R_i increases monotonically such that by (2.2), ε_R decreases monotonically everywhere thereby excluding the possibility of any elastic unloading. Using this relation in (2.3) and integrating with the limits (2.4), one finds the following relation between σ^∞/σ_Y and R_0/R_i

$$\frac{\sigma^{\infty}}{\sigma_Y} = -2\int_1^{\infty} f\left[\frac{2}{3}\ln\left\{1-\frac{1-(R_i/R_0)^3}{\eta^3}\right\}\right]\frac{d\eta}{\eta}. \tag{2.5}$$

The cavitation limit stress $\sigma^{\infty} \equiv S$ is obtained from (2.5) by letting $R_0/R_i \to \infty$ as

$$S/\sigma_Y = -2\int_1^{\infty} f\left[\frac{2}{3}\ln\{1-\eta^{-3}\}\right]\eta^{-1}\,d\eta \tag{2.6}$$

$$= -\int_0^{\infty} [e^{3\xi/2}-1]^{-1} f(-\xi)\,d\xi. \tag{2.7}$$

The cavitation limit exists if $e^{-3\xi/2}f(-\xi)$ is integrable.

Consider an elastic–perfectly plastic material with Young's modulus E, tensile yield stress σ_Y, and an initial tensile yield strain $\varepsilon_Y = \sigma_Y/E$ so that

$$\sigma/\sigma_Y \equiv f(\varepsilon) = \varepsilon/\varepsilon_Y \quad |\varepsilon| \leqslant \varepsilon_Y$$
$$= \text{sign}(\varepsilon) \quad |\varepsilon| > \varepsilon_Y. \tag{2.8}$$

A direct evaluation of (2.7) gives

$$S/\sigma_Y = -\frac{2}{3}\int_0^1 \ln[1-e^{-3\varepsilon_Y\xi/2}]\,d\xi \tag{2.9}$$

$$= \frac{2}{3}\left\{1+\ln\left(\frac{2}{3\varepsilon_Y}\right)\right\}+O(\varepsilon_Y). \tag{2.10}$$

The approximation (2.10) is highly accurate for $\varepsilon_Y < 0.01$. It is obtained from the exact expression (2.9) using $1-\exp(-3\varepsilon_Y\xi/2) \cong 3\varepsilon_Y\xi/2$. Values of S/σ_Y from (2.9) are given in Table 1 under the column for $N = 0$.

The radius of the plastically deformed region, R_Y, satisfies

$$\ln\left(\frac{R_Y}{R_0}\right) = \frac{1}{2}\frac{\sigma^{\infty}}{\sigma_Y} - \frac{1}{3}. \tag{2.11}$$

TABLE 1. *Values of* $S/\sigma_Y(\nu = 1/2)$

	N			
ε_Y	0	0.1	0.2	0.3
0.001	5.00	6.86	9.90	14.99
0.002	4.54	6.00	8.27	11.88
0.003	4.27	5.52	7.42	10.34
0.005	3.93	4.95	6.44	8.65

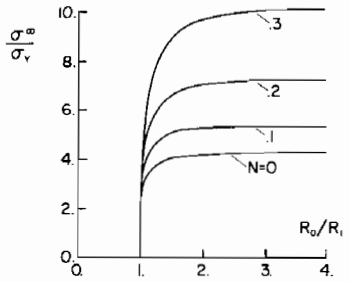

FIG. 1. Remote stress vs radius of the cavity for spherically symmetric loading. Results are shown for an elastic–perfectly plastic solid and for 3 levels of strain hardening, in each case with $\sigma_Y/E = 0.003$.

In the limiting cavitation state, by (2.10),

$$R_Y/R_0 \cong (3\varepsilon_Y/2)^{-1/3}. \tag{2.12}$$

Formulae (2.10) and (2.12) are given by HILL (1950). The plastic zone has a fixed size relative to the current size of the cavity (typically 4 to 8 times the current radius of the cavity, depending on ε_Y). Outside the plastic zone is an elastic field in which the strains diminish to zero as R^{-3}. The cavitation stress S becomes unbounded in the limit of a rigid–perfectly plastic solid (i.e. as $\varepsilon_Y \to 0$ when $E \to \infty$).

Next consider a power-law hardening solid with

$$\sigma/\sigma_Y \equiv f(\varepsilon) = \varepsilon/\varepsilon_y \quad |\varepsilon| \leqslant \varepsilon_Y$$
$$= \text{sign}\,(\varepsilon)(|\varepsilon|/\varepsilon_Y)^N \quad |\varepsilon| > \varepsilon_Y, \tag{2.13}$$

where again $\varepsilon_Y = \sigma_Y/E$. Values of S/σ_Y obtained numerically from (2.7) are included in Table 1 for $N = 0$ (the elastic–perfectly plastic limit (2.9)), 0.1, 0.2 and 0.3. The full relation of σ^∞/σ_Y versus R_0/R_i from (2.5) is plotted in Fig. 1 for $\varepsilon_Y = 0.003$ and the same four N-values. The cavitation limit stress is approached rapidly and is effectively attained once the void has expanded to about three times its original radius.

When the material is elastically compressible the analysis is not so simple but some specific results can be obtained (HILL, 1950; HUANG, 1989). In particular the limit yield stress for the elastic–perfectly plastic solid with Poisson's ratio ν is

$$\frac{S}{\sigma_Y} = -\frac{2}{3\alpha}\ln\{1-\alpha e^{-(1+\nu)\varepsilon_Y}\}$$
$$+\frac{2(1-\nu)}{(1+\nu)\varepsilon_Y}\int_0^{(1+\nu)\varepsilon_Y}\xi[(1+\nu)(e^\xi-1)+2(1-2\nu)\xi]^{-1}\,d\xi, \tag{2.14}$$

where $\alpha = 1-2(1-2\nu)\varepsilon_Y$. With terms of order ε_Y and smaller neglected, (2.14) is

$$\frac{S}{\sigma_Y} = \frac{2}{3}\left\{1+\ln\left(\frac{1}{3(1-\nu)\varepsilon_Y}\right)\right\}. \tag{2.15}$$

3. AXISYMMETRIC CAVITATION STATES: ELASTIC REMOTE REGION

Axisymmetric stressing is considered such that the non-zero remote stresses are

$$\sigma_{33}^\infty = S, \quad \sigma_{11}^\infty = \sigma_{22}^\infty = T. \tag{3.1}$$

Attention is limited to isotropic elastic–perfectly plastic solids characterized by a

Mises yield condition in the form $\sigma_e = \sigma_Y$, where σ_e is an effective stress invariant defined below and σ_Y is the tensile flow stress. In this section we investigate cavitation under conditions where the remote field remains elastic. Specifically, the stresses in the remote field are limited to the range

$$S - \sigma_Y < T \leqslant S. \tag{3.2}$$

Thus, one end of the range, $T = S$, corresponds to the spherically symmetric problem of the previous section. At the other end of the range, $S - T = \sigma_Y$, yielding occurs remotely, and this limit will be dealt with separately in the next section.

In the range of remote stressing specified by (3.2), the solution procedure couples an outer elastic solution to a finite strain, elastic–plastic solution in an inner region which contains the yielded material surrounding the void. As described below, Lagrangian multipliers are used to couple an analytical representation for the outer solution to a finite element representation of the solution in the inner region.

3.1. *Outer solution: elastic field*

Large strain effects are of no consequence in the outer elastic field because the material under consideration is assumed to have an initial yield strain, $\varepsilon_Y \equiv \sigma_Y/E$, no greater than about 10^{-2}. Let R^* be the radius of the spherical surface which separates the inner and outer regions, such that all yielding is confined well within the domain $R < R^*$. The following velocities satisfy the field equations for axisymmetric deformations of a linear isotropic elastic solid (LUR'E, 1964):

$$\begin{aligned} v_r &= \frac{1}{E}[(1-\nu)\dot{T} - \nu\dot{S}]R\sin\phi - B_0 R^{-2}\sin\phi - C_0 R^{\ 2}\left[\frac{9}{4}\sin 3\phi - \frac{1}{4}(11-16\nu)\sin\phi\right], \\ v_z &= \frac{1}{E}[\dot{S} - 2\nu\dot{T}]R\cos\phi - B_0 R^{\ 2}\cos\phi - C_0 T^{-2}\left[\frac{9}{4}\cos 3\phi + \frac{1}{4}(31-32\nu)\cos\phi\right]. \end{aligned} \tag{3.3}$$

Here $z \equiv x_3$ and $r \equiv (x_1^2 + x_2^2)^{1/2}$ are axial and planar-radial coordinates, and ϕ is the azimuthal angle measured from the z-axis. The traction components acting on the surface ($R = R^*$) of the inner region are

$$\begin{aligned} \dot{T}_r &= \dot{T}\sin\phi + B_0 R^{-3}\dot{T}_r^{\mathrm{B}}(\phi) + C_0 R^{-3}\dot{T}_r^{\mathrm{C}}(\phi), \\ \dot{T}_z &= \dot{S}\cos\phi + B_0 R^{\ 3}\dot{T}_z^{\mathrm{B}}(\phi) + C_0 R^{-3}\dot{T}_z^{\mathrm{C}}(\phi), \\ (\dot{T}_r^{\mathrm{B}}, \dot{T}_z^{\mathrm{B}}) &= 4G(\sin\phi, \cos\phi), \\ \dot{T}_r^{\mathrm{C}} &= 2G[9\sin 3\phi - (1-2\nu)\sin\phi], \\ \dot{T}_z^{\mathrm{C}} &= 2G[9\cos 3\phi + (11-4\nu)\cos\phi], \end{aligned} \tag{3.4}$$

where $G = E/(2(1+\nu))$ is the shear modulus.

The origin of the lead terms in (3.3) and (3.4) is obvious. The additional terms have free amplitude factors B_0 and C_0 which will be used to couple the outer elastic field to the solution in the inner region. The above representation of the outer solution

neglects terms in the velocities which decay with large R like R^{-3} and faster. The terms with amplitude B_0 comprise the spherically symmetric contribution.

3.2. *Numerical method for the inner region and coupling with outer solution*

The analysis for the inner region is based on a Lagrangian formulation of the field equations, using a cylindrical reference coordinate system, in which $x^1(=r)$, $x^2(=\theta)$ and $x^3(=z)$ are the radial, circumferential and axial coordinates respectively. The Lagrangian strains are given by

$$\eta_{ij} = \tfrac{1}{2}(u_{i,j}+u_{j,i}+u^k_{,i}u_{k,j}), \tag{3.5}$$

where u^i are displacement components on the reference base vectors and ( ), denotes covariant differentiation in the reference frame. In this subsection, superscripts and subscripts are associated with contravariant and covariant components, respectively, according to the usual convention. The contravariant components of the Kirchhoff stress tensor τ^{ij} and the Cauchy stress tensor σ^{ij} are related by

$$\tau^{ij} = \sqrt{G/g}\sigma^{ij}, \tag{3.6}$$

where g and G are the determinants of the metric tensors g_{ij} and G_{ij} in the reference configuration and the current configuration, respectively. The equilibrium equations are expressed in terms of the principle of virtual work

$$\int_V \tau^{ij}\delta\eta_{ij}\,\mathrm{d}V = \int_A T^i\delta u_i\,\mathrm{d}A, \tag{3.7}$$

where V and A are the reference volume and surface, respectively, and T^i are the nominal traction components.

As mentioned earlier, attention is limited to isotropic elastic–perfectly plastic solids. Let $s^{ij} = \tau^{ij} - G^{ij}\tau^k_k/3$ be the components of the deviator of the Kirchhoff stress, and define an effective stress quantity as

$$\sigma_e = (3/2s^{ij}s_{ij})^{1/2}. \tag{3.8}$$

The strain rate for a plastic loading increment is taken to be

$$\dot{\boldsymbol{\varepsilon}} = \frac{1+\nu}{E}\overset{\nabla}{\boldsymbol{\tau}} - \frac{\nu}{E}(\overset{\nabla}{\tau^k_k})\mathbf{G} + \frac{\dot{\lambda}}{E}\mathbf{s}, \tag{3.9}$$

where $\overset{\nabla}{\boldsymbol{\tau}}$ is the Jaumann rate of the Kirchhoff stress and $\dot{\lambda}$ is non-negative. The plastic part of the strain rate is $\dot{\lambda}\mathbf{s}/E$ and this vanishes if $\sigma_e < \sigma_Y$ or if $\dot{\sigma}_e < 0$ when $\sigma_e = \sigma_Y$.

We have chosen to use the Kirchhoff stress rather than the Cauchy stress in the above formulation to gain the advantage for numerical work of a symmetric stiffness matrix for the resulting finite element equations. The differences in predictions based on the two formulations is expected to be very small, as is well known. Strictly speaking, the condition for remote yielding in terms of the true stress components S and T from (3.8) becomes $S-T = \sqrt{g/G}\sigma_Y$ rather than $S-T = \sigma_Y$. This small

distinction will be ignored since g/G departs from unity only due to elastic compressibility.

The multiaxial incremental stress–strain relationship is of the form $\dot{\tau}^{ij} = L^{ijkl}\dot{\eta}_{kl}$, with the tensor of instantaneous moduli given by

$$L^{ijkl} = \frac{E}{1+\nu}\left\{\frac{1}{2}(G^{ik}G^{jl}+G^{il}G^{jk})+\frac{\nu}{1-2\nu}G^{ij}G^{kl}-\beta\frac{3}{2}\frac{s^{ij}s^{kl}}{\sigma_Y^2}\right\}$$
$$-\frac{1}{2}(G^{ik}\tau^{jl}+G^{jk}\tau^{il}+G^{il}\tau^{jk}+G^{jl}\tau^{ik}). \quad (3.10)$$

Here, the value of β is 1 or 0 for plastic yielding or elastic unloading, respectively. Plastic yielding continues as long as $s^{ij}\dot{\eta}_{ij} \geqslant 0$. In the numerical solution the stress values on the yield surface are adjusted radially after each increment, so that the yield condition remains exactly satisfied.

The void considered is taken to be spherical initially with radius R_i, and the inner region analysed numerically is a concentric spherical region with initial radius R^*. Due to symmetry about the mid-plane $z = 0$ only half of the inner spherical region needs to be analysed numerically. Quadrilateral finite elements were used. These were comprised of four triangular linear displacement elements.

The displacement increments and the nominal traction increments on the surface of the inner region must agree with the values specified by the outer solution (3.3) and (3.4). In the incremental form of the principle of virtual work (3.7) geometrical compatibility with the outer solution is enforced by using a Lagrange multiplier method, thus adding the last two surface integrals in the following incremental variational equation

$$\int_V \{\dot{\tau}^{ij}\delta\eta_{ij}+\tau^{lj}\dot{u}_{,l}^{k}\delta u_{k,j}\}\,\mathrm{d}V-\int_A \dot{T}^i\delta u_i\,\mathrm{d}A-\int_A \delta\lambda_r[\dot{u}_1-\dot{u}_r^0]\,\mathrm{d}A$$
$$-\int_A \delta\lambda_z[\dot{u}_3-\dot{u}_z^0]\,\mathrm{d}A = 0. \quad (3.11)$$

On the surface $R = R^*$ the expressions for $\dot{T}_i$, $\dot{u}_r^0$ and $\dot{u}_z^0$ specified by the outer solution are substituted into (3.11), while the displacement fields $\dot{u}_i$ in the spherical inner region are represented in terms of the finite element approximation.

A convenient choice for the variations of the Lagrangian multipliers is

$$\delta\lambda_r = \delta B_0 R^{-3}\dot{T}_r^{\mathrm{B}}(\phi)+\delta C_0 R^{-3}\dot{T}_r^{\mathrm{C}}(\phi), \quad (3.12)$$

$$\delta\lambda_z = \delta B_0 R^{-3}\dot{T}_z^{\mathrm{B}}(\phi)+\delta C_0 R^{-3}\dot{T}_z^{\mathrm{C}}(\phi). \quad (3.13)$$

These expressions are substituted into (3.11), together with the outer solution expressions for the displacement increments and traction increments on the surface of the spherical inner region. This choice preserves the symmetry of the matrix system. With the finite element approximation of the displacement increments in the inner region, the variational equation (3.11) gives $N+2$ linear algebraic equations, where the first N unknowns are the nodal displacement increments and the last two unknowns are the integration constants B_0 and C_0 in the outer solution.

All solutions to be presented here are started from a uniform stress state equal to that specified at infinity. Since the outer solutions rely on the assumption of small deviations from this uniform stress state, initial equilibrium is ensured by specifying this stress state in the inner region. Subsequently, equilibrium is enforced by the incremental solution. To avoid drifting away from the true equilibrium path standard equilibrium correction terms are applied at all nodal points inside the outer surface (e.g. see TVERGAARD and NEEDLEMAN, 1984). The initial loads applied to the spherical void surface in order to obtain the uniform stress state are subsequently stepped down over a number of increments until the void surface is free of tractions.

Two calculation procedures were used to calculate the values of S and T associated with the cavitation states. The more direct procedure was the less effective of the two. It entailed fixing the ratio T/S and incrementing S, once the initial loads on the void surface were stepped down to zero. The normalized growth rate of the void, $\dot{V}/(\dot{\varepsilon}V)$, where $\dot{\varepsilon}$ is the remote axial strain rate, becomes unbounded as S approaches the cavitation limit. This procedure had poor numerical stability as the cavitation limit was approached and was not very useful for accurately determining the cavitation instability limit.

The effective procedure capitalized on the nature of the cavitation limit as an eigenstate. Now, values of S and T are prescribed to be fixed throughout the computation. The loads on the void surface are taken to be proportional to a load parameter λ which was an initial value $\lambda = 1$ in the uniform initial state. The normalized growth rate of the void, $\dot{V}/\dot{\lambda}$, is monitored as λ is reduced. If $\dot{V}/\dot{\lambda}$ becomes unbounded before λ reaches zero, the remote stresses lie outside the cavitation limit. Then in the next computation S and T must be scaled down. If, on the other hand, $\dot{V}/\dot{\lambda}$ only becomes unbounded when λ is negative (corresponding to loads pushing out on the void surface), the remote stresses lie within the cavitation limit and must be scaled up in the next computation. In this way, the instability limit can be narrowed down by a sequence of computations. In carrying out the above procedure it proved to be expedient to use the displacement of the equatorial radius as the prescribed quantity which is incremented in the computation with $\dot{\lambda}$ as a calculated quantity. This is simply an exchange in the roles of these two quantities in the system of linear algebraic equations for the incremental quantities.

3.3. *Numerical results: remote stressing in the elastic range*

The computed cavitation states are presented in Fig. 2 in the form of curves of S/σ_Y and σ_m/σ_Y versus $(S-T)/\sigma_Y$ for $\varepsilon_Y \equiv \sigma_Y/E = 0.003$ and $\nu = 0.3$. Here σ_m/σ_Y is the measure of the triaxiality of the remote stress where the mean stress is

$$\sigma_m \equiv \tfrac{1}{3}\sigma_{kk} = \tfrac{1}{3}(S+2T). \tag{3.14}$$

The nonlinear scale for variation with T/S is also shown on the abscissa. The value of S/σ_Y only varies from 4.06 when $S = T$ (the spherically symmetric limit) to 4.54 as $(S-T)\sigma_Y \to 1$. The corresponding variation of the mean stress is even smaller. Thus in this range cavitation is approximately controlled by a critical value of either the *mean stress* or the *maximum principal stress S*.

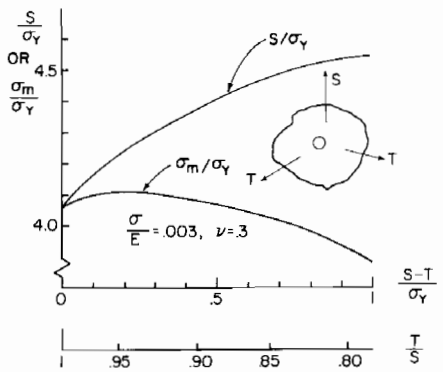

FIG. 2. Cavitation limits for a void in an elastic–perfectly plastic material subject to remote axisymmetric stressing. Shown are the critical values of the remote mean stress, σ_m/σ_Y, and the remote maximum principal stress, S/σ_Y, as a function of the combination of S and T.

The cavitation state $S/\sigma_Y = 4.06$ in the spherically symmetric limit ($S = T$) was calculated independently using the numerical procedure described above giving agreement with the analytical result (2.15) to within a small fraction of a per cent. This close agreement provides a check on the numerical procedure, including the coupling of the numerical solution for the inner region with the closed form solution for the outer region.

Most of the numerical computations leading to Fig. 2 were carried out with a ratio of the initial coupling boundary radius R^* to void radius R_i of $R^*/R_i = 100$. At the onset of the cavitation instability the void has grown so the current value of this radius has decreased. Nevertheless, except when $S-T$ is nearly σ_Y, the choice $R^*/R_i = 100$ is more than adequate to ensure that the plastic region is contained well within the inner region. In fact, when $(S-T)/\sigma_Y$ is relatively small, calculations carried out with $R^*/R_i = 10$ were in close agreement with those obtained using $R^*/R_i = 100$. The largest value of $(S-T)/\sigma_Y$ for which calculations were made with the elastic outer solution was approximately 0.98. In this instance $R^*/R_i = 1000$ was used, and the maximum radius of the plastic zone had grown to about 30 times the current average void radius in the cavitation state.

The shape of the void in the cavitation state departs only slightly from spherical. For example, with $(S-T)/\sigma_Y = 0.75$ the void in the cavitation state is slightly oblate with an aspect ratio of approximately 0.97. Oblate shapes under high triaxiality were documented in earlier studies of asymptotic void shapes in rigid–plastic solids (BUDIANSKY and HUTCHINSON, 1980). Although we have not attempted any calculations with initial void shapes other than spherical, it seems unlikely that the cavitation limit should depend significantly on the starting shape, at least for shapes which do not differ drastically from being spherical. In any case, in the range of remote stress states represented in Fig. 2 the shape used at the start of the calculation is very close to that attained in the cavitation state.

4. AXISYMMETRIC CAVITATION STATES: PLASTIC REMOTE REGION

Now consider the elastic–perfectly plastic solid characterized in the previous section remotely stress to yield with

$$S-T=\sigma_{\mathrm{Y}}, \tag{4.1}$$

and, as before, let

$$\frac{\sigma_m}{\sigma_{\mathrm{Y}}}=\frac{S+2T}{3\sigma_{\mathrm{Y}}}, \tag{4.2}$$

be the measure of stress triaxiality, where σ_m is the remote mean stress. Plastic flow now occurs in the remote field with the strain rates approaching

$$\dot{\varepsilon}_z=-2\dot{\varepsilon}_r=-2\dot{\varepsilon}_\theta\equiv\dot{\varepsilon}, \tag{4.3}$$

as $R\to\infty$.

At high triaxiality a void with an initially spherical shape rapidly evolves to an asymptotic shape which is slightly oblate. The normalized dilatation rate of the void, $\dot{V}/(\dot{\varepsilon}V)$, where V is the current volume of the void, depends on σ_{Y}/E, $\sigma_{\mathrm{m}}/\sigma_{\mathrm{Y}}$ and ν, i.e.

$$\dot{V}/(\dot{\varepsilon}V)=F(\sigma_{\mathrm{Y}}/E,\sigma_m/\sigma_{\mathrm{Y}},\nu). \tag{4.4}$$

For reference we recall the RICE–TRACEY (1969) high triaxiality approximation to the normalized dilatation rate for a spherical void in an incompressible, *rigid*–perfectly plastic solid ($\sigma_{\mathrm{Y}}/E=0$)

$$[\dot{V}/(\dot{\varepsilon}V)]_0=0.850\exp[3/2(\sigma_m/\sigma_{\mathrm{Y}})]. \tag{4.5}$$

No cavitation limit exists for a rigid–plastic solid, but (4.5) displays the extremely strong dependence of the dilatation rate on stress triaxiality.

In this section we present results for the normalized dilatation rate for *elastic*–perfectly plastic solids. We show that this rate becomes unbounded as $\sigma_m/\sigma_{\mathrm{Y}}$ approaches the cavitation limit and we calculate this cavitation limit for specific values of σ_{Y}/E. The numerical solution procedure parallels those described in the previous section except that the outer region must be modified to represent the field of a solid which is remotely at yield. The representation of the solution in the inner region is still taken to be that in Section 3.2.

4.1. *Outer solution: plastic field*

In the limit $R\to\infty$ the stresses approach

$$\sigma_z=S,\quad \sigma_r=\sigma_\theta=T \tag{4.6}$$

together with the yield condition (4.1). The remote strain rate $\dot{\varepsilon}$ is prescribed with (4.3) holding as $R\to\infty$. The approximation of the solution in the outer region uses the lowest order perturbation of the stress increments and velocities in the remote field. The perturbation is developed as a rigorous expansion of the equations of the finite deformation formulation in Section 3.2. It is outlined in the Appendix. Because the remote stresses approach uniform values, the lowest order perturbation problem for the increments of stress and velocities reduces to a problem for a solid with homogeneous, transversely isotropic instantaneous moduli. The form of the velocities in the outer field is

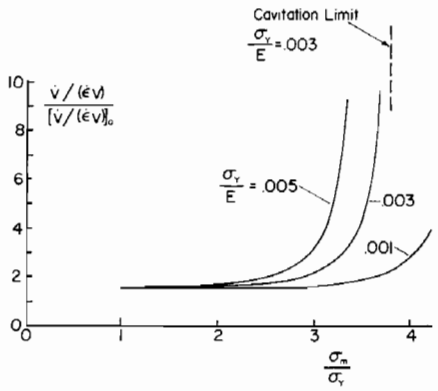

FIG. 3. Influence of cavitation limit on the normalized dilatation rate for an elastic–perfectly plastic solid which is remotely yielded ($S-T=\sigma_Y$, $\nu=0.3$). Here $\dot{\varepsilon}$ is the remote strain-rate and $[\dot{V}/(\dot{\varepsilon}V)]_0$ is the high triaxiality approximation (4.5).

$$v_r = -\tfrac{1}{2}\dot{\varepsilon}R\sin\phi + B_0R^{-2}v_r^B(\phi) + C_0R^{-2}v_r^C(\phi),$$
$$v_z = \dot{\varepsilon}R\cos\phi + B_0R^{-2}v_z^B(\phi) + C_0R^{-2}v_z^C(\phi), \tag{4.7}$$

where R and ϕ are spherical coordinates in the current configuration. The $v(\phi)$s depend on σ_Y/E, σ_m/σ_Y and ν as well as ϕ, as specified in the Appendix. The contribution with amplitude B_0 is no longer spherically symmetric. The associated nominal traction rates on the spherical surface with radius $R = R^*$ have the form

$$\dot{T}_i = \dot{\varepsilon}\dot{T}_i^0(\phi) + B_0R^{-3}\dot{T}_i^B(\phi) + C_0R^{-3}\dot{T}_i^C(\phi). \tag{4.8}$$

4.2. *Dilatation rates and cavitation states*

The normalized dilatation rates presented in Fig. 3 were computed using the coupled inner and outer representations. The calculations were initiated with uniform tractions specified over the initially spherical void surface consistent with (4.6). These tractions are stepped down to zero simultaneously with the imposition of increments of remote strain $\dot{\varepsilon}$. The normalized dilatation rate, $\dot{V}/(\dot{\varepsilon}V)$, is calculated using the current volume V somewhat after the point where the tractions on the void surface have been eliminated when the void is still nominally spherical. The rate in Fig. 3 has been scaled by the rigid–plastic approximation (4.5) to reveal the cavitation limit, independently of its strong dependence on mean stress. Included in Fig. 3 is the result of a direct calculation of the cavitation limit of $\sigma_Y/E = 0.003$ and $\nu = 0.3$ which will be described below and which gave $\sigma_m/\sigma_Y = 3.78$ ($S/\sigma_Y = 4.45$).

Well below the cavitation limit (e.g. $\sigma_m/\sigma_Y \leqslant 2$) the dilatation rate is only weakly dependent on σ_Y/E and scales with the rigid–plastic approximation (4.5). In this range our results do exceed the widely used high triaxiality approximation (4.5) by more than 50%. This discrepancy is a consequence of inaccuracy in the approximate formula (4.5). This matter is addressed separately from the issue of cavitation instabilities in Section 6.

undeformed radius of the wire, u is the displacement across the crack faces, σ is the nominal stress (the load carried by the specimen divided by the cross-sectional area of the undeformed wire, πa_0^2), and $\sigma_Y = 5.3$ MPa is a measure of the initial tensile yield stress of the unconstrained wire.

Little or no debonding between the lead wire and the glass was observed to occur in the specimens whose load–deflection behavior is shown in Fig. 5. Consequently, the constraint imposed by the glass cylinder on the wire was fully maintained as is reflected by the very large values of σ/σ_Y achieved in the test. These specimens failed by the enlargement of a *single* void in the wire somewhere on or near the plane of the crack. An example of the final failure surface from ASHBY *et al.* (1989) is shown in Fig. 6 where it can be seen that the void grew to encompass about one half the cross-sectional area of the wire. The remaining annular ligament failed by shearing off. The initial size of the void, or the size of the particle from which it nucleated, is not known but is presumably on the scale of microns. Its final size is a fraction of a millimeter, and thus its volume has increased by a factor of more than 10^6.

ASHBY *et al.* (1989) present uniaxial stress–strain curves for the unconstrained lead wire material. The material displayed fairly high strain hardening and considerable variation from one uniaxial curve to another. Using representations for their uniaxial curves in the form $\sigma/\sigma_Y = f(\varepsilon)$, we have evaluated the cavitation limit for spherically symmetric stressing from (2.7). (The piecewise power-law (2.13) does not adequately fit the stress–strain curves. We have used a more complicated representation which more closely reproduces the measured data.) The computed spherically symmetric cavitation limit ranged from $S/\sigma_Y = 6$ to $S/\sigma_Y = 7.5$, depending on which set of uniaxial tensile data was used. The state of stress in the wire where cavitation occurred was almost certainly at yield and not spherically symmetric. Nevertheless, the results of the previous section suggest that the cavitation stress predicted for the spherically symmetric state should be a reasonable estimate for the present application. The high constraint and exceptionally high values of σ/σ_Y ensure that $\sigma \cong \sigma_m$. The peak values of σ/σ_Y recorded experimentally in Fig. 5 do fall within, or a little below, the predicted range for the cavitation limit for most of the specimens.

6. DILATATION RATES

It was noted in connection with the results in Fig. 3 that the widely used high triaxiality approximation (4.5) of RICE and TRACEY (1969) underestimates the dilatation rate by more than 50% even well below the cavitation limit. The curves of Fig. 3 are reproduced in Fig. 7 along with results for the normalized dilatation rate of a spherical void in a rigid–perfectly plastic solid.

The results shown in Fig. 7 for the dilatation rate of a spherical void in a rigid–perfectly plastic solid have been recomputed (HUANG, 1989) along the lines originally detailed in RICE and TRACEY (1969) and BUDIANSKY *et al.* (1982). Considerable effort has been taken in recomputing the rigid–perfectly plastic results to ensure that the number of functions used to represent the velocity field leads to a converged result for the dilatation rate. Details of these calculations will be published elsewhere. The main finding, seen in Fig. 7, is that the widely used high triaxiality approximation

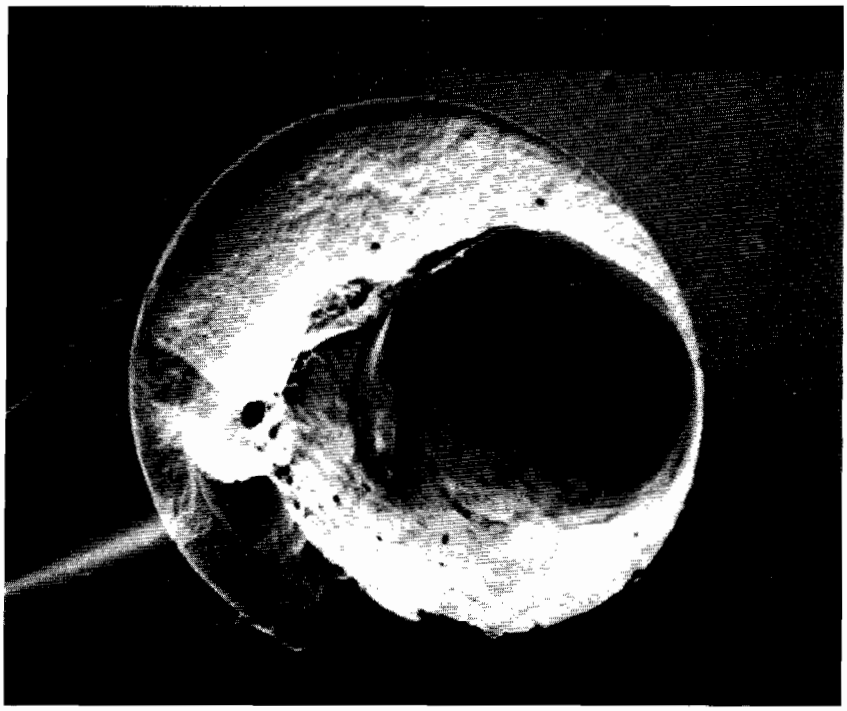

FIG. 6. A photograph from ASHBY *et al.* (1989) showing the failure mode of the well bonded wires. A single void grows until it occupies almost one half the cross-section of the wire and the remaining ligament shears off.

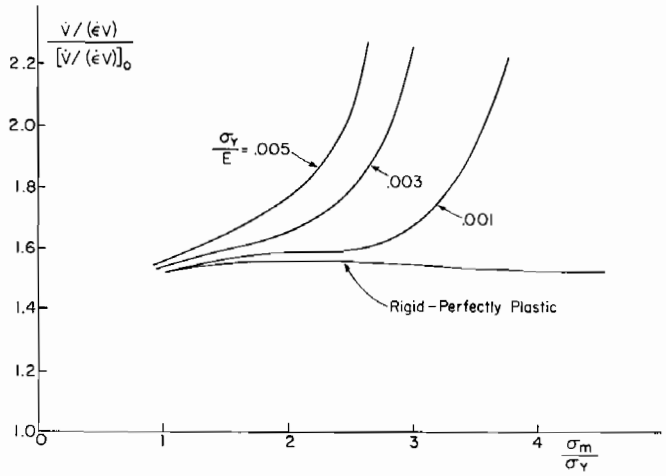

FIG. 7. Effect of elasticity on the dilatation rate of nominally spherical voids. The high triaxiality approximation, $[\dot{V}/(\dot{\epsilon}V)]_0$, in (4.5) is used as a normalizing reference.

(4.5) underestimates the dilatation rate of the void by more than 50% at all levels of triaxiality above $\sigma_m/\sigma_Y = 1$. Moreover, elasticity comes into play at triaxialities in the range of σ_m/σ_Y from 1 to 2. As is evident from Fig. 7, the existence of the cavitation instability for the elastic–perfectly plastic solid manifests itself even in the lower triaxiality range. For $\sigma_Y/E = 0.003$ (a typical value), the dilatation rate is more than 60% higher than the high triaxiality approximation when σ_m/σ_Y exceeds unity. At triaxiality levels above $\sigma_m/\sigma_Y = 2$, the influence of the cavitation instability begins to dominate and the formula is even more in error.

Researchers have noted that the high triaxiality formula (4.5) tends to underestimate experimentally measured growth rates by amounts comparable to those seen in Fig. 7 (BEREMIN, 1981). Recently in a numerical study of the growth rate of a spherical void near the tip of a crack, HOM and MCMEEKING (1989) found that the void grew at roughly twice the rate expected from the high triaxiality formula (4.5). This was attributed to interaction with the crack tip, but is likely to be due, in part, to inaccuracy inherent in the formula.

ACKNOWLEDGEMENTS

This work was supported in part by the National Science Foundation (Grant No. MS-88-12779), the Materials Rescarch Laboratory (Grant No. NSF-DMR-86-14003) and the Division of Applied Sciences, Harvard University.

REFERENCES

ABEYARATNE, R. and HOU, H.-S. 1989 *J. appl. Mech.* **56,** 40.
ASHBY, M. F., BLUNT, F. J. and BANNISTER, M. 1989 *Acta Metall.* **37,** 1857.

BALL, J. M.	1982	*Phil. Trans. R. Soc.* (Lond.) **A306,** 557.
BEREMIN, F. M.	1981	*Advances in Fracture Research*, ICF5, **2,** 809.
BISHOP, R. F., HILL, R. and MOTT, N. F.	1945	*Proc. Phys. Soc.* **57,** 147.
BUDIANSKY, B. and HUTCHINSON, J. W.	1980	In *Proc. XVth Int. Cong. Theoretical and Applied Mechanics* (Postprints) (edited by F. P. J. RIMROTT and B. TABARROK). North-Holland, Amsterdam.
BUDIANSKY, B., HUTCHINSON, J. W. and SLUTSKY, S.	1982	*Mechanics of Solids, The Rodney Hill 60th Anniversary Volume* (edited by H. G. HOPKINS and M. J. SEWELL), p. 13. Pergamon Press, Oxford.
CHADWICK, P.	1959	*Q. Jl. Mech. appl. Math.* **12,** 52.
DALGLEISH, B. J., TRUMBLE, K. P. and EVANS, A. G.	1989	*Acta Metall.* **37,** 1923.
DURBAN, D. and BARUCH, M.	1976	*J. appl. Mech.* **43**, 633.
ELLIOTT, H. A.	1948	*Proc. Camb. Phil. Soc.* **44,** 522.
HILL, R.	1950	*The Mathematical Theory of Plasticity*. Clarendon Press, Oxford.
HOM, C. L. and MCMEEKING, R. M.	1989	*J. Mech. Phys. Solids* **37,** 395.
HUANG, Y.	1989	Ph.D. thesis, work in progress.
LUR'E, A. I.	1964	*Three-Dimensional Problems in the Theory of Elasticity* (edited by J. R. M. RADOK). Interscience, New York.
ORTIZ, M. and MOLINARI, A.	1989	Effect of strain hardening and rate sensitivity on the dynamic growth of a void in a plastic material, to be published.
RICE, J. R. and TRACEY, D. M.	1969	*J. Mech. Phys. Solids* **17,** 201.
TVERGAARD, V. and NEEDLEMAN, A.	1984	*Acta Metall.* **32,** 157.

APPENDIX

Outer solution : plastic field

Let r and z be radial and axial coordinates of a material point in the current configuration and let $R = (r^2+z^2)^{1/2}$ be the distance from the origin. Write the velocities in the outer field as

$$\mathbf{v} = \mathbf{v}^{\infty} + \hat{\mathbf{v}}, \tag{A1}$$

where

$$v_r^{\infty} = -\dot{\varepsilon}r/2 \quad \text{and} \quad v_z^{\infty} = \dot{\varepsilon}z \tag{A2}$$

with $\hat{\mathbf{v}}$ as the lowest order perturbation from the uniform field which decays to zero as $R \to \infty$. Since the remote stresses approach uniform values, $\boldsymbol{\sigma}^{\infty}$, given by (3.1), the relation between the stress rates and the strain rates in the remote field is given by the constitutive relation of Section 3.2 where $\mathbf{L}$ in (3.10) is evaluated using $\boldsymbol{\sigma}^{\infty}$. Let $\dot{n}_{ij}$ be incremental components of the nominal stress with respect to fixed Cartesian axes so that incremental equilibrium is specified by

$$\dot{n}_{ij,i} = 0. \tag{A3}$$

With the aid of well-known connections between the several stress rates, one can use the constitutive relation to obtain

$$\dot{n}_{ij} = c_{ijkl} v_{l,k}, \tag{A4}$$

where explicit expressions for the cs are readily identified which depend on E, ν, S and T. These instantaneous moduli are homogeneous and transversely isotropic with respect to the z-axis.

Following a procedure laid out by ELLIOTT (1948), one can represent the axisymmetric velocity field $\hat{\mathbf{v}}$ by two velocity potentials $\Phi_i(r, t)(i = 1, 2)$ such that in cylindrical coordinates

$$\hat{v}_r = \frac{\partial}{\partial r}(\Phi_1 + \Phi_2) \quad \text{and} \quad \hat{v}_z = \frac{\partial}{\partial z}(k_1\Phi_1 + k_2\Phi_2), \tag{A5}$$

where k_1 and k_2 are specified below. The potentials satisfy

$$\frac{\partial^2\Phi_i}{\partial r^2} + \frac{1}{r}\frac{\partial\Phi_i}{\partial r} + m_i\frac{\partial^2\Phi_i}{\partial z^2} = 0 \quad (i = 1, 2), \tag{A6}$$

where m_1 and m_2 are the roots of

$$m^2\{(C_{11} - T)(C_{44} - (S - T)/2)\} + m\{(C_{13} + C_{44} - (S + T)/2)^2 - (C_{11} - T)(C_{33} - S) - C_{44}^2 + ((S - T)/2)^2\} + (C_{33} - S)(C_{44} + (S - T)/2) = 0 \tag{A7}$$

and

$$C_{11} = K + G, \quad C_{12} = K - G,$$
$$C_{13} = C_{33} = K, \quad C_{44} = G$$

with $G = E/(2(1+\nu))$ and $K = E/(3(1-2\nu))$. The ks are given by

$$k_i = \{(C_{11} - T)m_i - (C_{44} + (S - T)/2)\}/(C_{13} + C_{44} - (S + T)/2). \tag{A8}$$

The two roots m_i are complex conjugates of one another, as are the k_i. The general solution for Φ_1, leading to velocities which decay at infinity, is

$$\Phi_1 = \sum_{n=0}^{\infty} A_n R_1^{-(n+1)} P_n(\cos\phi_1), \tag{A9}$$

where the A_n are complex, $P_n(x)$ is the nth order Legendre Polynomial and

$$R_1 = (r^2 + z^2/m_1)^{1/2}, \quad \cos\phi_1 = z/(R_1\sqrt{m_1}). \tag{A10}$$

The general solution for Φ_2 is the complex conjugate of Φ_1, so that the velocities from (A5) are real. Only the first term, $n = 0$, in (A9) is used in the representation for the outer field. The terms with $n \geqslant 1$ give rise to velocities contributions which decay faster than R^{-2} for large R. The free amplitudes B_0 and C_0 introduced in Section 4 enter (A9) as $A_0 = B_0 - iC_0$.